Scattering Patterns of Self-Assembled Cubic Phases. 1. The Model

Piotr Garstecki and Robert Hołyst*

Institute of Physical Chemistry, Polish Academy of Sciences, Department III, Kasprzaka 44/52, 01-224 Warsaw, Poland

Received August 15, 2001

Bragg reflection amplitudes are examined for the structures P, D, G, C(P), C(D), I-WP, and F-RD in amphiphilic systems. For these ordered phases, a very simple analytical formula for the scattering amplitudes is given. The formula allows determination of the scattering amplitudes for any cross-sectional density profile of the membrane decorating the minimal surface. Within this approximation an analytical solution for the Debye−Waller factor is presented. Finally we propose a simplified model that can greatly facilitate examination of the experimental scattering patterns.

1. Introduction

The self-assembling systems form a wide variety of structures on the mesoscopic scale. The amphiphilic nature of surfactants and lipids induces a very complex behavior in mixtures with water and hydrocarbons. Depending on the thermodynamic and structural parameters of the system, such as temperature, composition, or length of an aliphatic chain in a surfactant molecule, many different structures can be formed. The basic structures forming at low concentrations of surfactants are the spherical micelles, cylinders, and plane surfaces. At higher concentrations these structures can order as follows: micelles on the cubic lattice, cylinders on the 2D hexagonal lattice, and plane membranes in lamellar phases. In a thin range of parameters, the amphiphilic molecules arrange in the cubic liquid crystal phases made of curved bilayers (inverse phase) or two distinct continuous channels separated by a water film (direct phase) (Figure 1). These phases display the highest degree of organization and therefore attracted a lot of theoretical and experimental interest.

There are only few different theoretical proposals for the construction and analysis of these phases. One is the rod model introduced by a pioneer in the field of X-ray scattering from self-assembled systems (Luzzati[1]). His idea is as follows: One constructs a continuous channels out of straight rods joined at specific angles and coordination numbers characteristic for each cubic structure. A more common, current, approach is based on the assumption that the curved layers (made of either amphiphilic molecules (inverse phase) or water (direct phase)) decorate the triply periodic minimal surfaces (TPMSs) (Figure 1). The surface divides the space into two channels that consist of the same type of molecules (Figure 1). The TPMS had already been known in the 19th century. The first one, the double diamond, D surface, was discovered by Schwartz in 1865.[2] Since then a number of TPMSs have been discovered by Alan Schoen[3] and also obtained numerically by the minimization of the Landau−Ginzburg functionals in real space.[4] The surfaces that have been found in real systems are the D, P, and G surfaces, discovered on the basis of the symmetry from X-ray spectra and diffusion measurements indicating the existence of channels spanning the structures. Some authors suggested

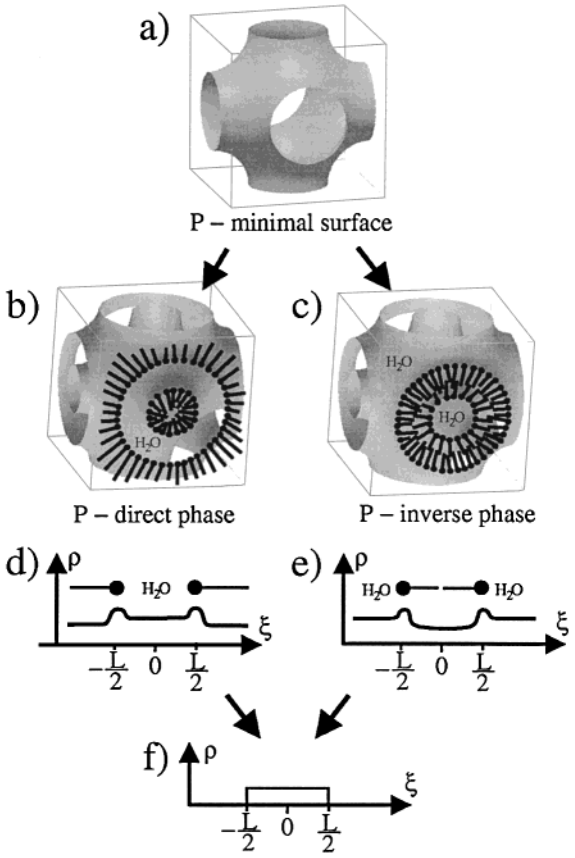

Figure 1. (a) The zero width mathematical surface in the unit cell of the P structure. The TPMS can be decorated by a water film (b, direct phase) or by a lipid bilayer (c, inverse phase). These phases lead to different cross sectional density profiles (d and e), respectively. Still, in the first step approximation of the small-angle X-ray scattering intensity, these profiles can be modeled by (f) a uniform density distribution. See text for explanation.

* Corresponding author. E-mail: holyst@saka.ichf.edu.pl, http://www.ichf.edu.pl/Dep3.html.

(1) Luzzati, V.; Spegt, P. A. *Nature* **1967**, *215*, 701−703.

(2) Schwartz, H. A. *Monatsber. Koniglichen Akad. Wissenscaften Berlin* **1865**, 149−153.

(3) Schoen, A. H. Infinite Periodic Minimal Surfaces without Self-intersections; NASA Technical Note TD-5541, 1970.

(4) Góźdź, W. T.; Hołst, R. *Phys. Rev. E: Stat. Phys., Plasmas, Fluids, Relat. Interdiscip. Top.* **1996**, *54*, 5012−5029.

10.1021/la011298p CCC: $22.00
Published on Web 03/09/2002

also the existence of other cubic phases based on TPMS, for example, the F-RD[5] and Neovius C(P) surfaces.[6]

Despite the long and already quite rich history of both the theoretical and experimental studies of TPMSs, there is still a significant need for clear and straightforward structural analysis procedures. The X-ray diffractograms are used almost only for the symmetry characterization, and the lack of simple formulas for the scattering intensities hampers further analysis of the X-ray data. The lack of simple theoretical tools is only one of the reasons for the incomplete analysis of the X-ray data. Usually the X-ray (or neutron) data contain only a few visible peaks and therefore contain much less information than the X-ray spectra obtained for crystalline solids. The structural complexity of the TPMSs makes the theoretical studies difficult and computationally demanding. Another difficulty comes from the fact that a unit cell of the cubic structures contains a large number of molecules: thousands of surfactants and hydrocarbons and tens or hundreds of thousands water molecules. Unfortunately typical programs for the analysis of the X-ray diffraction patterns work well for less than 200 molecules in a unit cell.

Nevertheless there have been a number of theoretical analyses of the scattering from TPMS. As a first step in the analysis, one finds a scattering amplitude for the TPMS without any decorating layer.[7,8] Still the data give only the structure factors of these surfaces and thus cannot be directly compared with experimental spectra, which are strongly influenced by the width of the layer decorating TPMS. An example of a comparison between theory and experiment involving the molecular factor (MF) associated with the width of the water or surfactant layer is the very elegant work of Clerc and Dubois-Violette.[9] The authors presented an isotropic model of the MF and fitted the experimental data for several G surface based systems. Although the fits were very promising, they were done only for the decorated G surface and its applicability for other structures has not been confirmed. Only recently a beautiful work in this field has been done by Harper and Gruner.[10,11] They have presented a detailed calculation of the scattering amplitudes for real lipid bilayers. From the data, the authors have been able to reconstruct the bilayer's cross sectional density from the scattering intensities, assuming the reduction of the density for the terminal CH_3 methyl groups. Unfortunately their analysis is rather complex, and therefore it is not an easy and computationally simple tool for the analysis of the X-ray data.

The purpose of this paper is to fill this apparent gap in the theoretical studies and provide a simple tool for the theoretical analysis of the experimental data for the cubic periodic structures formed in the water mixtures of surfactants with hydrocarbons.

In this work a set of data for each cubic structure is given in a simple analytical form. The subsequent article presents applications of our tool to various experimental systems and specific predictions concerning the structure and kinetics of their phase behavior.

The paper is organized as follows. Section 2 contains a description of the system and the main result of the paper. The three following sections deal with the structure factors, molecular factors, and Debye−Waller factors of the P, D, G, C(P), C(D), I-WP, and F-RD structures. A summary of our work can be found in section 6.

2. The Basic Result: Analytical Formula

The cubic phases made from the self-assembled surfactant molecules with hydrocarbon chains in water solutions can be physically realized in two possible ways. One is a direct phase in which a water film is centered on the triply periodic minimal surface (in case of the C(P), C(D), F-RD, and I-WP, the TPMS is modeled here as a nodal surface[12]), while the two disjoint subspaces are filled with surfactant molecules (Figure 1b). The second possibility is an inverse phase where the TPMS is decorated by a surfactant bilayer and the two channels are filled with water (Figure 1c). In each case, knowing the microscopic details of the molecules present in the system, one can postulate the form of the cross sectional electron density profile $\rho(\xi)$ in the direction normal to the surface. A schematic drawing of these profiles for a direct and an inverse phase is illustrated in parts d and e of Figure 1. It is a good question whether a one-dimensional density profile contains all of the information on the density distribution within a three-dimensional cubic cell. It does when two assumptions are fulfilled. One is that the regions of a given species (surfactant heads, tails, or water molecules) are contained within so-called parallel surfaces (surfaces of a constant distance to the base minimal surface). Another possibility is that the bounding surfaces are the constant curvature ones. It is a subject of an ongoing dispute which of these two postulates is true. Still, as argued in ref 10, these two solutions are quite close to each other and assuming parallel surfaces should not introduce significant deviations. The second assumption is that the one-dimensional density profile does not change within the cubic cell. This is generally true due to the nature of the lipid or surfactant bilayers which are two-dimensional fluids. Since the molecules can freely move along the membrane, any density fluctuations should be leveled on a very short time scale. There still remains the dependence of the density profile on the local curvature which is not constant. Reference 11 contains a detailed study of this problem. Yet reconstructing the detailed density profiles requires an analysis that starts with fitting the spectra with amplitudes for a constant density distribution. Furthermore as it will be argued below and shown in our following paper that these matters will not affect the procedure leading to the determination of the most crucial parameters of a cubic phase. The last effects having an impact on the scattering amplitudes are the fluctuations of the membrane. They will be discussed in detail in the fifth section. For now it is enough to point out that characteristic relaxation times of both the molecular and collective fluctuations of the membrane are by many orders of magnitude shorter than typical exposition times in the scattering experiments. Thus it is enough to account for the fluctuations by introducing another parameter σ into the expression for the average density distribution. As shown in the following sections, despite of the geometrical complexity of the TPMS-based cubic phases, all of these effects factorize and the scattering amplitude can be expressed as a product of a structure

(5) Maddaford, P. J.; Toprakcioglu, C. *Langmuir* **1993**, *9*, 2868−2878.
(6) Landh, T. *J. Phys. Chem.* **1994**, *98*, 8453−8467.
(7) Mackay, A. L. *Nature* **1985**, *314*, 604−606.
(8) Anderson, D. M.; Davies, H. T.; Scriven, L. E.; Nitsche, J. C. C. *Adv. Chem. Phys.* **1990**, *77*, 337−396.
(9) Clerc, M.; Dubois-Violette, E. *J. Phys. II* **1994**, *4*, 275−286.
(10) Harper, P. E.; Gruner, S. M. *Eur. Phys. J. E* **2000**, *2*, 217−228.
(11) Harper, P. E.; Gruner, S. M.; Lewis, R. N. A. H.; McElhaney, R. N. *Eur. Phys. J. E* **2000**, *2*, 229−245.
(12) Schwartz, U. S.; Gompper, G. *Phys. Rev. E: Stat. Phys., Plasmas, Fluids, Relat. Interdiscip. Top.* **1999**, *59*, 5528−5541.

Table 1. Data from Numerical Evaluations[a]

TPS	χ	s_0*
P	−4	2.3458
D	−2	1.9192
G	−8	3.0966
C(D)	−30[b]	4.4921
C(P)	−16	3.7519
F-RD	−40	4.8580
I-WP	−12	3.5543

[a] χ is the Euler characteristic per unit cell and $s_0^* = s_0/a^2$ is the dimensionless surface area of the TPS per unit cell with the cell parameter a. [b] The value obtained by the Euler relation for a triangulated surface. Please note that the best reconstruction of the volume fraction ϕ (eq 7) and surface area of the parallel surfaces $s_{||}$ (eq 8) is obtained for $\chi = -36$. It is the same value as reported by Landh.[6]

factor F^S, molecular factor F^M, and the Debye−Waller factor F^{DW}:

$$A(\mathbf{q}, \rho(\xi), \sigma) = F^S(\mathbf{q})\, F^M(\mathbf{q}, \rho(\xi))\, F^{DW}(\mathbf{q}, \sigma) \qquad (1)$$

The main result of this paper is summarized by the following formula

$$A(\mathbf{q}\neq 0, \rho(\xi), \sigma) = F^S[2\int_0^\infty \mathrm{d}\xi'\, \rho(\xi') \cos(q\alpha_{hkl}\xi')] \exp\left[-\frac{1}{2}(q\alpha_{hkl}\sigma)^2\right] \qquad (2)$$

where ξ is the distance away from the base minimal surface, $\mathbf{q} = (2\pi/a)[h,k,l]$ is the scattering wave vector ($q = (2\pi/a)(h^2 + k^2 + l^2)^{1/2}$), h, k, l are the Miller indices, and σ is a standard deviation related to the fluctuations amplitude (see section 5). The normalized structure factors and the α parameters are explicitly given in Tables 2−8 for the P, D, G, C(P), C(D), F-RD, and I-WP TPMS based cubic phases. Thus *this formula allows an evaluation of the scattering amplitudes for any density profile $\rho(\xi)$ and fluctuations parametrized by the standard deviation σ.* The model scattering intensity for the powder samples is

$$I(\mathbf{q}, \rho(\xi), \sigma) = \mathcal{M}_{hkl}|A(\mathbf{q}, \rho(\xi), \sigma)|^2 \qquad (3)$$

where the multiplicity factor $\mathcal{M}_{hkl}$ is also included in the tables. *This method provides an easy to use tool which facilitates a very detailed determination of the actual cross sectional density profiles in the amphiphilic cubic systems.*

It is important to point out that expression 2 sets the normalization of the amplitudes in which the amplitude of the 000 reflection is equal to the total contrast electron density within the unit cell

$$A(\mathbf{q}=0) = \int_0^\infty \mathrm{d}\xi\, \rho(\xi)[2s_0^* a^2 + 4\pi\chi\xi^2] \qquad (4)$$

where a is the cubic cell parameter and $s_0^* = s_0/a^2$ is the dimensionless surface area of the base minimal surface per unit cell and is given by the structure factor for the 000 reflection ($s_0 = F^S_{000}$). The term in brackets gives the surface area of the parallel surfaces inclosing the sub-volume of the layer decorating the base TPMS (see eq 8). Both the surface areas of the base TPMS and their Euler characteristics χ per unit cell are summarized in Table 1.

In many cases an even simpler analysis is needed. The cubic phases formed in self-assembling systems have a growing potential for nanomaterial investigations and possible industrial applications. There, the key features of these phases such as their type (direct−inverse) and the layer width, L, are of crucial importance. For example in catalytic applications the size of the pores has a dramatic influence on the efficiency and molecular selectiveness of the material. Since the main contrast is associated with the density difference between water and hydrocarbons, it is legitimate to assume a flat density profile for both cases (Figure 1f). In the scattering experiments only the intensity is measured, therefore the sign of the density difference can also be neglected and only the width L of the layer decorating the TPMS is important. Furthermore, as will be shown in the fifth section, the fluctuations of the membranes have a minor influence on the relative intensity of the hkl peaks when compared with the influence of the layer width. Thus inserting a flat density profile $\rho(\xi)$ eq 11 and $\sigma = 0$ into eq 2, we obtain

$$A(\mathbf{q}\neq 0, L) = F^S \frac{2\rho_0}{\alpha_{hkl} q} \sin\left(\alpha_{hkl} q \frac{L}{2}\right) \qquad (5)$$

where ρ_0 is the electron density within the layer and

$$A(\mathbf{q}=0, L) = \rho_0\, \phi(L^*)\, a^3 \qquad (6)$$

where ϕ is the volume fraction of the layer (see eq 7). We will show in the following article that this simplified modeling leads to a good approximation for the intensity of the Bragg reflections and provides a very valuable insight into the details of the cubic phase structure.

Fitting of the model intensities given by substituting amplitude eq 5 into eq 3 to the experimental intensities provides the layer width L. To compute area per surfactant head for the direct and inverse structure of a given layer width L, one can use the following formulas which relate the dimensionless layer width $L^* = L/a$ with the volume fraction of the layer ϕ and the surface area of the interface between surfactant and water-rich regions $s_{||}^* = s_{||}/a^2$:

$$\phi = s_0^* L^* + \frac{\pi}{6}\chi L^{*3} \qquad (7)$$

$$s_{||}^* = 2s_0^* + \pi\chi L^{*2} \qquad (8)$$

In most cases, comparison of the areas per surfactant head for the direct and inverse phase enables determination of which of the types has been formed. An example of such analysis is presented in our following paper.

3. The Structure Factor

The structure factor (SF) arises from the base TPMS. It is given by

$$F^S = \int_S \mathrm{d}^2\mathbf{r} \exp[i\mathbf{q}\mathbf{r}] \qquad (9)$$

where the integral is taken over the base minimal surface within the unit cell. To calculate the SF, the surfaces have been triangulated. Then the integral over the surface has been substituted by a sum over the centers of the triangles

$$F^S = \sum_{j=1}^{N} s_j \exp[i\mathbf{q}\mathbf{r}_j] \qquad (10)$$

where s_j is the jth triangle's surface area and r_j is the location of its center of mass. This procedure has been described in detail in our previous paper.[13] The structure factors for the 000 reflection give the surface area s_0 of the base TPMS. Thus the SFs have the dimension of surface

(13) Garstecki, P.; Hołst, R. *J. Chem. Phys.* **2000**, *113*, 3772−3779.

area. Table 1 summarizes the computed areas for the seven explored structures.

The lists of all of the SFs for the strongest Bragg reflections are included in Tables 2−8. As shown in ref 13, they are in a very good agreement both with the space symmetry group of the explored structures and with analytical evaluations for the P, D, and G surfaces conducted by Mackay,[7] Anderson,[8] and Clerc and Dubois-Violette.[9]

Values of the surface area of the base TPS for the C(P), C(D), F-RD, and I-WP structures are slightly different than those given in the literature. For example for the C(P) TPS, we obtain a value of $s_0^* = 3.7519$ while Anderson[8] provides $s_0^* = 3.510$. Still our value is very close to the one established by Schwartz[12] ($s_0^* = 3.809$). These differences might be caused by the fact that Anderson has worked with minimal surfaces, while Schwartz (as in this work) has used its nodal approximation.

4. The Molecular Factor

To evaluate the formula for a molecular factor (MF), we have first performed calculations for a flat cross sectional density profile (see Figure 1f)

$$\rho(\xi) = \rho_0 \Theta\left(\frac{L}{2} - \left|\xi\right|\right) \tag{11}$$

where ρ_0 is the density within the layer, Θ is the Heaviside step function ($\Theta(x) = 0$ for $x < 0$ and $\Theta(x) = 1$ for $x > 0$), ξ is a coordinate along the direction normal to the base minimal surface, namely, it is the distance away from the minimal surface, and, finally, L is the width of the layer. Apart from the layer, the density is set to zero; thus the integral over the whole volume of the unit cell can be substituted by an integral over the subvolume inclosed between the parallel surfaces

$$A(\mathbf{q}, L) = \int_V \mathrm{d}^3\mathbf{r}\rho(\xi(\mathbf{r}))\exp[i\mathbf{qr}] = \rho_0 \int_{V:\xi(\mathbf{r})|<L/2} \mathrm{d}^3\mathbf{r}\exp[i\mathbf{qr}] \tag{12}$$

To perform this last integral numerically, the unit cell of each TPMS has been projected on a cubic grid $N \times N \times N$ of size up to $N = 96$ for the D surface, $N = 128$ for G and C(D), and $N = 192$ (P, C(P), I-WP, and F-RD). For each point j on the grid, the smallest distance d_j to the surface has been calculated. Then the integral eq 12 has been evaluated as a sum over points laying in a distance d smaller than $L/2$ from the TPMS

$$A(\mathbf{q}, L) = \frac{\rho_0 a^3}{N^3} \sum_{j:d_j<L/2} \exp[i\mathbf{qr}_j] \tag{13}$$

A schematic visualization of this procedure is shown in Figure 2c. To check the accuracy of this method, we have performed calculations for two analytically accessible structures—a vesicle and a rotational sinusoid. The results of these tests are presented in the following subsection.

4.1. A Vesicle and a Rotational Sinusoid. Lets imagine a single layer of vesicles arranged on a 2D square lattice in the xy plane. It is important to remember here that it serves only as an abstract test structure for our model. Still this kind of thin layer of vesicles made from amphiphilic molecules has been obtained experimentally.[14]

(14) Velev, O. D.; Gurkov, T. D.; Ivanov, I. B.; Borwanka, R. P. *Phys. Rev. Lett.* **1995**, *75*, 264−267.

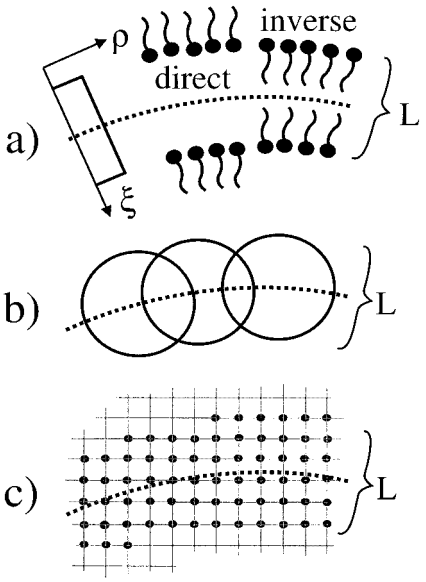

Figure 2. Visualization of the models used to evaluate the scattering intensities: (a) schematic view of the base surface decorated by either water film (direct phase) or lipid bilayer (inverse phase) and the assumed density profile; (b) the isotropic model; (c) the lattice model. See text for explanation.

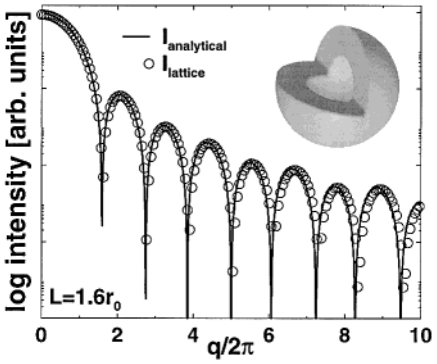

Figure 3. The scattering intensity as a function of the scattering vector length for a single layer of vesicles arranged on a 2D square lattice. The insert presents the vesicle.

The vesicle is constructed by decorating a sphere of radius $r_0 = a/4$ with a layer of uniform density and width ranging from $L = 0$ to $L = a/2$. The analytical expression for the scattering amplitude reads

$$A^{\mathrm{ves}}(\mathbf{q}, L) = \frac{1}{L}\int_0^{2\pi} \mathrm{d}\phi \int_0^{\pi} \mathrm{d}\theta \sin\theta \int_{r_0+L/2}^{r_0-L/2} \mathrm{d}r\, r^2 \exp[i2\pi lr\cos\theta] \tag{14}$$

where for simplicity the lattice cell parameter has been set to unity ($a = 1$) and the scattering vector $\mathbf{q} = (2\pi/a)[h,k,l]$ is parallel to the z axis ($h = 0$ and $k = 0$). Figure 3 presents the scattering intensity as a function of the scattering wave vector. The lattice model reproduces the intensity evaluated analytically very well.

The sphere is a structure of positive Gaussian curvature (both principal radii of curvature have the same sign). The TPMSs have negative Gaussian curvature meaning that at every point on the surface, the principal radii of curvature have opposite signs. Thus we have used another test structure that has both positive and negative Gaussian curvature regions. It is a rotational sinusoid (Figure 4). Its base surface is a cylinder of radius $a/4$ modulated by a sinus function. In the cylindrical coordinates the base

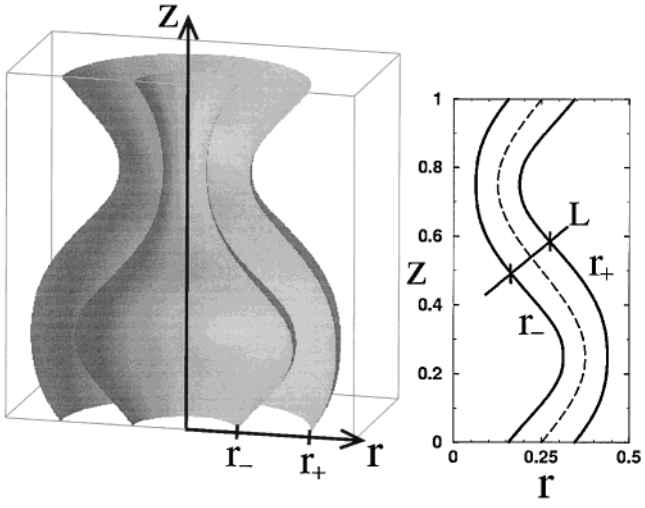

Figure 4. A cut through a unit cell of a rotational sinusoid. The structure is periodic in the *z* direction and is arranged on a 2D square lattice in the *xy* plane.

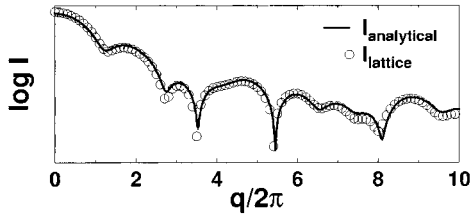

Figure 5. A comparison of the scattering intensity calculated analytically and numerically using the lattice model for a rotational sinusoid for the scattering vector equal to $\mathbf{q} = q(2\pi/a)[1, 1, 1]$.

surface is given by the following equation

$$r = \frac{a}{4} + \frac{a}{8}\sin(2\pi z) \tag{15}$$

Again the base surface is decorated by a layer of uniform density and width $L \in (0, a/4)$. These kinds of structures have been proposed for the intermediate stage in the kinetics of phase transitions between hexagonal and cubic structures (see for example (ref 15)). The scattering amplitude

$$A^{\sin}(\mathbf{q}, L) = \frac{1}{L}\int_0^1 \mathrm{d}z \int_0^{2\pi} \mathrm{d}\phi \int_{r_-}^{r_+} \mathrm{d}r\, r \exp[i\mathbf{qr}] \tag{16}$$

where r_- and r_+ are functions of z setting the boundaries of the layer in such a way that the layer width L is constant in the direction normal to the surface of the sinusoid. Figure 5 presents the comparison of the scattering intensity obtained analytically and numerically for the scattering vector $\mathbf{q} = q(2\pi/a)[1,1,1]$ and $L = a/4$. Again the lattice model reproduces it very well.

4.2. The Isotropic Fit. Our goal is to find a form of the expression for the scattering amplitude (eq 12) that would factorize into a product of a structure factor and a molecular factor

$$A(\mathbf{q}, L) = F^{\mathrm{S}}(\mathbf{q})F^{\mathrm{M}}(\mathbf{q}, L) \tag{17}$$

Dividing the left-hand side of this equation (obtained numerically (eq 13)) by the appropriate structure factor, we can extract an effective MF which was then fitted by a simple formula.

(15) Shi, A. *J. Phys.*: *Condens. Matter.* **1999**, *11*, 10183−10197.

It appeared that the simple formula can be extracted from the model[9] shown in (Figure 2b). In its original form it was first proposed by Clerc and Dubois-Violette[9] and was successfully used to fit several scattering patterns of the simple gyroid, G, structure based phases. The idea is to decorate the TPMS with spheres of radius $L/2$ of a uniform density on the surface. This leads to an isotropic MF independent of the local curvature and orientation of the surface

$$F^{\mathrm{M}}_{\mathrm{iso}} = \frac{2}{qa}\sin(qL/2) \tag{18}$$

This model reconstructs the Heaviside function form of the scattering density in the direction normal to the surface only for plane surfaces. In the case of the curved surfaces, it is only an approximation which fails when the local radius of curvature is comparable with the layer width L.

We have found that for the uniform density distribution within the layer, the effective MFs of the explored TPMS-based cubic phases can be very well approximated by a slightly corrected isotropic factor

$$F^{\mathrm{M}}(\mathbf{q}, L) = \frac{2\rho_0}{\alpha_{hkl}q}\sin\left(\alpha_{hkl}q\frac{L}{2}\right) \tag{19}$$

where the correction parameters α_{hkl} are characteristic for every Bragg reflection and are explicitly given for the most prominent reflections for the P, D, G, C(P), C(D), F-RD, and I-WP structures in Tables 2−8. In this notation the MF has a dimension of electron charge per surface area. When multiplied by the SF of dimension of the area gives the final dimension of the scattering amplitude in arbitrary scale of electron charge. Please note here that it is exactly this form of the MF that has been inserted into the expression for the amplitude within the simplified model eq 5.

The details of fitting the isotropic MF to numerically obtained amplitudes are summarized in the following subsection.

4.3. Results for Triply Periodic Surfaces. A typical powder diffraction pattern of a cubic phase in a binary or ternary mixture consists of a few peaks. The number of the visible Bragg reflections rarely exceeds 10. To present the MFs for each structure, we have chosen a certain number of the most pronounced reflections. To enter the list, each peak had to be among the 10 strongest ones for any layer volume fraction $\phi \in (0, \phi_{\mathrm{limit}})$, where ϕ_{limit} was chosen to be equal to 0.8 for the P, D, G, and I-WP structures, 0.65 for F-RD and C(D), and 0.5 for C(P). The layer's volume fraction ϕ is related to the layer width L by eq 7.

In the case of the P, D, and G structures, the isotropic model works very well. The intensity dependence on the layer width L evaluated using this model is (except for a few peaks) the same as that given by the numerical integral eq 13. However for the C(P), C(D), I-WP, and F-RD surfaces, the numerical results differ significantly from the isotropic approximation and significant corrections (in terms of α_{hkl}) are needed in this case. A possible physical interpretation of the α_{hkl} parameters is the effective layer width seen in the cross section in the given *hkl* direction.

4.3.1. The Schoen P Surface. The P surface has the $Im\bar{3}m$ symmetry group, its surface area per cubic cell is $s_0^* = 2.3458$ and Euler characteristic $\chi = -4$. The P minimal surface is shown at the top of Figure 1. Table 2 contains the structure factors for the minimal surface for the 20 most prominent Bragg reflections. Almost all of the examined reflections are very well described by the

Table 2. The Scattering Data for the P Structure[a]

hkl	$\mathcal{M}_{hkl}$	$F_{hkl}{}^{S}$*	α_{hkl}
0 0 0	1	2.3458	
1 1 0	12	−0.4496	1.14
2 0 0	6	−0.5444	1
2 1 1	24	0.4565	1.03
3 1 0	24	0.0985	1
2 2 2	8	−0.4056	1
3 2 1	48	−0.2177	1
4 0 0	6	0.2454	1
4 1 1	24	−0.2425	1
3 3 0	12	0.2155	1
4 2 0	24	0.1580	1
3 3 2	24	0.2795	1
4 2 2	24	0.2536	1
5 2 1	48	0.0861	1
4 3 3	24	−0.2680	1
5 3 0	24	−0.1693	1
5 3 2	48	−0.1356	1
6 1 1	24	0.1577	1
5 4 1	48	0.1449	1
5 4 3	48	0.1795	1
5 5 4	24	−0.2070	1

[a] The first column contains the *hkl* indices, the second the appropriate multiplicity factors for a powder spectrum, the third the dimensionless structure factors $F^{S}* = F^{S}/a^{2}$ for the zero-width base mathematical surface, and the fourth the α_{hkl} correction parameters for the isotropic MF.

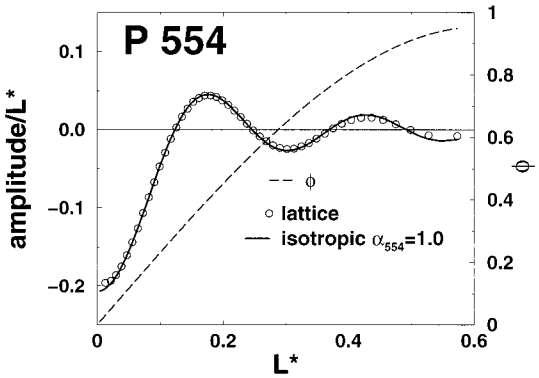

Figure 6. The P surface. The scattering amplitude of the 554 reflection plotted as a function of the dimensionless layer width $L^* = L/a$, where a is the cubic cell parameter. The amplitude computed via the lattice (numerical) model is drawn with open circles and the amplitude given by the isotropic fit with $\alpha_{554} = 1.0$ with a solid line. The dashed line gives the layer volume fraction ϕ as a function of L^*, eq 7. The amplitude has been divided by L^* in order to compare it with the structure factor $(A(\mathbf{q}, L)/L^* \rightarrow F^{S}*$ when $L^* \rightarrow 0)$.

uncorrected isotropic model. An example is shown in Figure 6. Even for large layer widths, the isotropic MF reproduces the numerically evaluated amplitude very accurately. Still two of the chosen peaks have to be slightly corrected. As an example we have plotted the amplitude of the 110 reflection as a function of the layer width L. To fit this dependence the isotropic MF required, the alpha parameter $\alpha_{110} = 1.14$ (see Figure 7). The same figure contains the values of the 110 amplitude for three specific layer widths L computed by Harper.[10] As in the case of all the other 11 peaks presented there,[10] the values are in excellent agreement with our computations.

Figure 8 shows how drastically the MF changes the relative intensities. One could imagine a binary water/surfactant system of a fixed volume composition 0.3/0.7. If the P phase has been formed, the direct phase would have the layer volume fraction $\phi \approx 0.3$ (upper diffraction pattern), while for the invert phase $\phi \approx 0.7$ (lower diffraction pattern). Thus comparing the numerical spectra

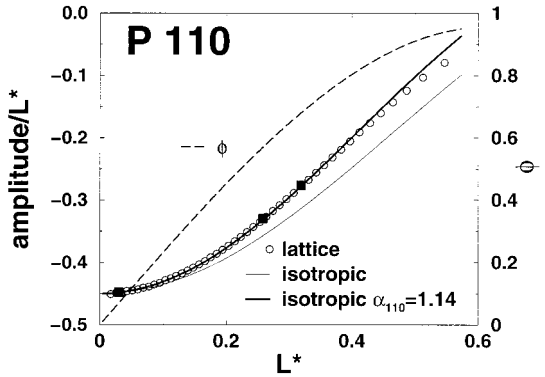

Figure 7. The P surface. The amplitude of the 110 reflection. The amplitude computed with the uncorrected isotropic MF is shown with the thin solid line while the corrected ($\alpha_{110} = 1.14$) fit is drawn with a thick solid line. The filled squares represent the amplitudes computed by Harper[10] for three volume fractions $\phi = 0.0766$, 0.5791, and 0.6998. As in the case of all the other 12 reflections presented in ref 10, the data are in very good agreement with the amplitudes computed via the lattice model (open circles). The layer volume fraction ϕ is given by the thick dashed line.

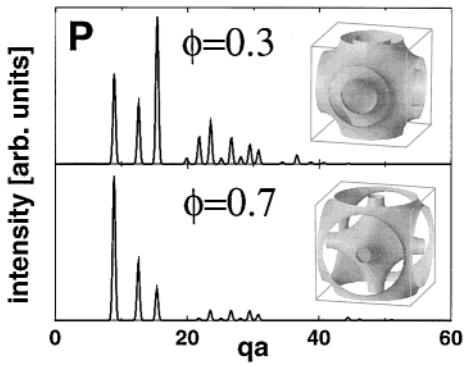

Figure 8. The scattering patterns for the P surface based cubic phases. The upper plot corresponds to the layer volume fraction $\phi = 0.3$ and the lower one to $\phi = 0.7$. The insets show the parallel surfaces within which the layer is confined.

with the experimental data, one can unambiguously determine which structure has been formed. This result in turn can lead to the determination of many microscopic (such as the area per surfactant head) and macroscopic (such as the phase stability) characteristics of the system.

4.3.2. The Schwartz D, Double Diamond Surface. The D surface (Figure 9) has $Pn\bar{3}m$ symmetry. It is worth noting here that this is a unit cell for the surface only, while the symmetry of the two subspaces ($Fd\bar{3}m$) requires an eight times bigger unit cell (two times bigger linear size of the unit cell). Since we consider the scattering with the surface contrast, it is enough to take smaller unit cell, for which $s = 1.9192$, $\chi = -2$. Again as in the case of the P structure, the effective MFs are very well described by the isotropic approximation. Only two reflections (110 and 200) display significant deviations from the isotropic model ($\alpha_{110} = 1.08$ and $\alpha_{200} = 1.09$). In the case of all the other chosen reflections, they are, within the numerical accuracy, equal to unity (see Table 3). Figure 10 shows the amplitude dependence on the layer width L for the 110 and 221 Bragg reflections.

4.3.3. The G, Gyroid Surface. The G surface (Figure 9) is of the $Ia\bar{3}d$ symmetry, $s = 3.0966$, $\chi = -8$. In Table 4 we present the results of our fits. For most of the 21 Bragg reflections, the isotropic model works excellently. Only four of the correction parameters differed more then

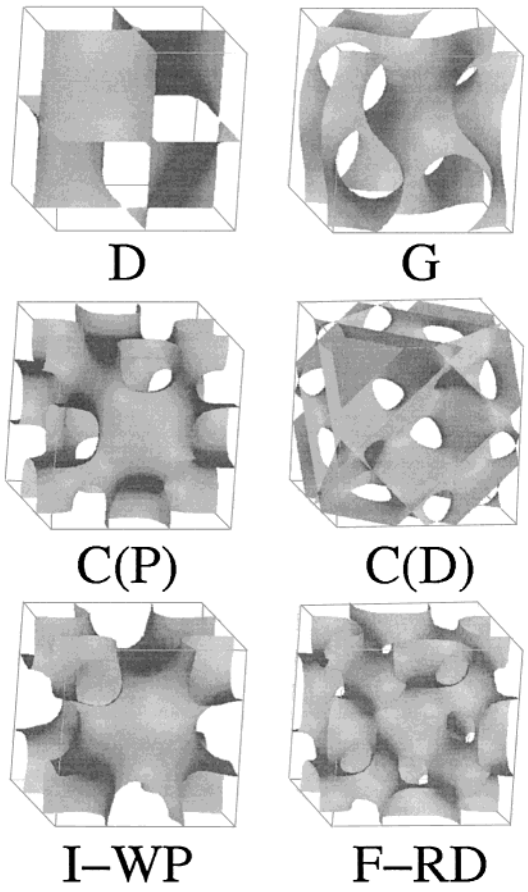

Figure 9. The unit cells of the minimal surfaces D and G and nodal surfaces C(P), C(D), I-WP and F-RD.

Table 3. The Scattering Data for the D Structure[a]

hkl	$\mathcal{M}_{hkl}$	F_{hkl}^{S*}	α_{hkl}
0 0 0	1	1.9192	
1 1 0	12	0.4794	1.08
1 1 1	8	0.4851	1
2 0 0	6	−0.2616	1.09
2 1 1	24	0.2120	1
2 2 0	12	0.2579	1
2 2 1	24	0.2799	1
3 1 0	24	−0.1885	1
3 1 1	24	−0.0987	1
2 2 2	8	0.2911	1
3 2 1	48	0.0957	1
3 2 2	24	0.1862	1
4 1 1	24	−0.1309	1
3 3 1	24	0.1812	1
4 2 0	24	−0.1436	1
4 2 1	48	−0.1084	1
3 3 2	24	0.2094	1
3 3 3	8	0.2203	1
4 3 2	48	0.1058	1
4 3 3	24	0.1600	1
4 4 2	24	0.1481	1
4 4 3	24	0.1722	1

[a] The legend is the same as for Table 2.

1% from unity ($\alpha_{211} = 1.07$, $\alpha_{220} = 0.97$, $\alpha_{321} = 1.04$, and $\alpha_{400} = 1.04$). Figure 11 presents the numerical data together with the isotropic fits for the 211 and 611 reflections.

4.3.4. The C(D), Complementary to D Surface. As in the case of the D structure for the surface contrast scattering computations, it is enough to take one-eighth of the cubic cell. The surface space group is $Pn\bar{3}m$. For the smaller cubic cell (Figure 9) the normalized surface area $s = 4.4921$ and the Euler characteristic $\chi = -30$. ($\chi = -36$ should be used to reconstruct the volume fraction ϕ of the layer and the surface area $s_{||}$ of the parallel surfaces.) Most of the 19 chosen reflections require corrections to the isotropic factor. Still the parameters α_{hkl} are sufficient to reconstruct the effective MF. The results for the C(D) structure are contained in Table 5.

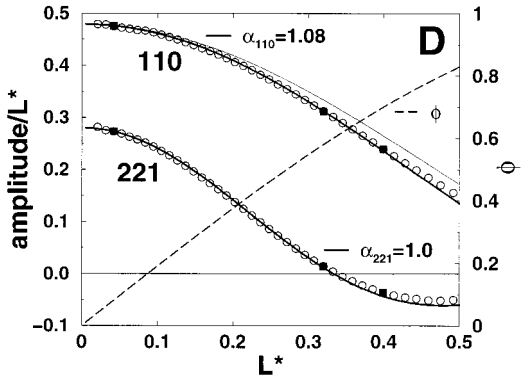

Figure 10. The D surface. The amplitudes of the 110 and 221 reflections. The lattice data are plotted with open circles. The filled squares present the amplitudes computed by Harper.[10] The amplitudes given by the isotropic model are drawn with solid lines. The thick lines correspond to the corrected MF ($\alpha_{110} = 1.08$ and $\alpha_{221} = 1.0$). In case of the 110 reflection, the uncorrected isotropic solution is shown (thin solid line). The layer volume fraction ϕ is given by thick dashed line.

Table 4. The Scattering Data for the G Structure[a]

hkl	$\mathcal{M}_{hkl}$	F_{hkl}^{S*}	α_{hkl}
0 0 0	1	3.0966	
2 1 1	24	0.6544	1.07
2 2 0	12	0.4306	0.97
3 2 1	48	−0.0971	1.04
4 0 0	6	−0.3375	1.04
4 2 0	24	−0.3309	1
3 3 2	24	0.4751	1
4 2 2	24	0.2770	1
4 3 1	48	0.1898	1
6 1 1	24	−0.2287	1
5 3 2	48	−0.1114	1
5 4 1	48	−0.1652	1
6 3 1	48	−0.1992	1
4 4 4	8	0.4112	1
5 4 3	48	0.3012	1
6 4 0	24	−0.1722	1
7 5 2	48	−0.1915	1
6 5 5	24	0.3112	1
6 6 4	24	0.2403	1
7 5 4	48	0.1700	1
7 7 6	24	0.2712	1
8 7 5	48	0.1715	1

[a] The legend is the same as for Table 2.

Figure 12 presents the results of fitting the isotropic form of the MF to the numerical data for the 111, 332, and 887 reflections.

4.3.5. The Neovius C(P), Complementary to P Surface. The C(P) surface (Figure 9) is of the same symmetry as the P structure ($Im\bar{3}m$). In our calculations we have obtained the surface area per cubic cell $s = 3.734$. The C(P)'s Euler characteristic is $\chi = -16$. Most of the C(P)'s 20 chosen peaks require corrections to the isotropic MF. The data for all of the peaks are included in Table 6.

4.3.6. The F-RD Surface. The F-RD structure (Figure 9) of the $Fm\bar{3}m$ symmetry has the surface area $s = 4.887$ and $\chi = -40$. Most of the 20 chosen peaks require significant corrections to the isotropic model. The reconstructed MFs fit the lattice model data very well. The data are presented in Table 7.

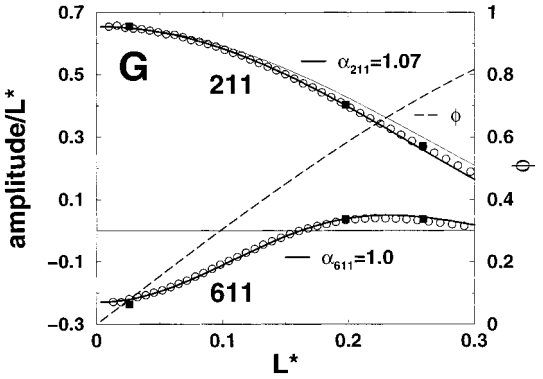

Figure 11. The G surface. A plot of the amplitudes of the 211 and 611 reflections. The legend is analogous to Figure 10.

Table 5. The Scattering Data for the C(D) Structure[a]

hkl	$\mathcal{M}_{hkl}$	$F_{hkl}{}^{S}$*	α_{hkl}
0 0 0	1	4.4921	
1 1 0	12	0.2228	1.88
1 1 1	8	−0.6489	1.69
2 0 0	6	−0.1303	0.84
2 1 1	24	−0.3337	1.13
2 2 1	24	−0.5483	1.14
3 2 1	48	−0.1474	0.92
4 0 0	6	0.2878	0.79
3 3 0	12	0.3785	1.09
3 3 2	24	0.3726	1
3 3 3	8	0.5463	1.05
4 3 2	48	0.1846	0.97
5 2 2	24	−0.2825	1.15
4 4 1	24	−0.2547	1
4 3 3	24	0.2765	1
6 3 3	24	0.3577	1.04
5 4 4	24	−0.3589	1
5 5 4	24	−0.3599	1
6 6 6	8	0.6251	1
8 8 7	24	−0.3430	1

[a] The legend is the same as for Table 2.

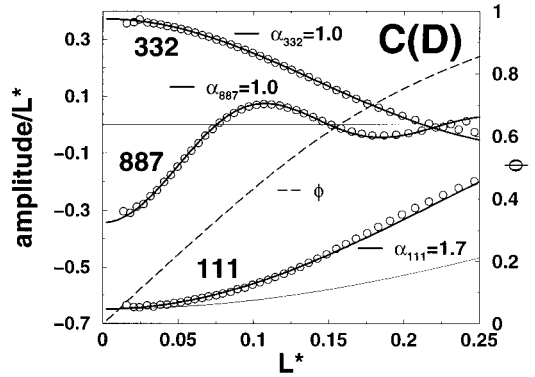

Figure 12. The C(D) surface. A plot of the amplitudes of the 111, 332, and 887 reflections.

4.3.7. The I-WP Surface. The I-WP surface (Figure 9) has the $Im\bar{3}m$ symmetry. In our calculations we have obtained a value of $s = S/a^2 = 3.554$ for the surface area per side of the cubic cell. Its Euler characteristic is equal to $\chi = -12$. All of the 21 selected peaks have been successfully fitted with the modified isotropic MF. The data are presented in Table 8. Figure 13 presents the fits for the 200 ($\alpha_{200} = 1.23$) and 400 ($\alpha_{400} = 0.98$) reflections.

4.3.8. Comment to the Results. The isotropic MF works very well for all three of the most commonly encountered structures, P, D, and G. Significant deviations from the isotropic model are seen when exploring the MFs of the more complex structures C(P), C(D), F-RD, and

Table 6. The Scattering Data for the C(P) Structure[a]

hkl	$\mathcal{M}_{hkl}$	$F_{hkl}{}^{S}$*	α_{hkl}
0 0 0	1	3.7519	
1 1 0	12	−0.5076	1.5
2 0 0	6	−0.3424	1.2
3 1 0	24	0.5250	1.02
2 2 2	8	−0.6448	1.09
3 2 1	48	0.1445	0.97
4 0 0	6	−0.4870	1.13
4 1 1	24	−0.4699	1.04
3 3 0	12	−0.4840	1.07
4 2 2	24	0.2527	0.97
5 2 1	48	−0.1448	1.0
6 0 0	6	0.4179	0.97
6 1 1	24	0.4737	0.97
7 1 0	24	−0.4532	1.0
5 5 2	24	0.2769	1.05
7 4 1	48	0.1796	1.0
8 3 1	48	−0.1889	1.0
9 1 0	24	0.3281	0.97
10 0 0	6	−0.6677	0.98
13 1 0	24	−0.3705	1.0

[a] The legend is the same as for Table 2.

Table 7. The Scattering Data for the F-RD Structure[a]

hkl	$\mathcal{M}_{hkl}$	$F_{hkl}{}^{S}$*	α_{hkl}
0 0 0	1	4.8580	
1 1 1	8	−0.4033	1.53
2 0 0	6	−0.8599	1.44
2 2 0	12	−0.5387	1.08
3 1 1	24	0.3002	1.25
3 3 1	24	0.2995	0.91
4 2 0	24	0.5770	1.03
4 2 2	24	−0.1075	0.96
3 3 3	8	−0.8719	1.05
5 1 1	24	−0.4983	1.06
4 4 0	12	−0.4920	1.13
5 3 1	48	−0.1255	0.92
6 0 0	6	−0.3637	1.03
6 2 0	24	0.2526	1.0
6 2 2	24	−0.3813	1.0
4 4 4	8	0.3859	1.0
7 1 1	24	0.5348	1.0
9 1 1	24	−0.3790	1.0
7 5 3	48	−0.2653	1.0
10 2 2	24	0.2699	1.0
12 2 0	24	−0.5034	0.99

[a] The legend is the same as for Table 2.

I-WP. This is caused by the fact that the normal vector distribution of the simple surfaces, P, D, and G, is very similar to that of the sphere. Thus the real MF, which should in general be a function of the local curvature and orientation of the vectors normal to the base surfaces, when averaged over the whole surface, gives similar results as the isotropic model without corrections. This is not true in the case of more complex structures, where the parameter α_{hkl} has to be used for almost all of the Bragg reflections.

4.4. The General Form of the Molecular Factor. Having the MF for a uniform density within the layer, one can compute the MF for a more complicated density profile. Lets imagine a structure composed of two thin layers of uniform density of scatterers ρ_0 of width Δl laying in a constant distance ξ from the minimal surface (see Figure 14). The cross sectional density distribution $\rho(\xi')$ of this structure can be written as a combination of two Heaviside functions

$$\rho(\xi') = \rho_0[\theta(\xi + \Delta\xi - |\xi'|) - \theta(\xi - |\xi'|)] \qquad (20)$$

For this density distribution, the amplitude is

Table 8. The Scattering Data for the I-WP Structure[a]

hkl	$\mathcal{M}_{hkl}$	$F_{hkl}{}^{S}$*	α_{hkl}
0 0 0	1	3.5543	
1 1 0	12	−0.2561	1.61
2 0 0	6	−0.5123	1.23
2 1 1	24	−0.0986	0.74
2 2 0	12	−0.5006	1.0
3 1 0	24	0.6608	1.05
2 2 2	8	0.3980	1.16
3 2 1	48	−0.0919	1.03
4 0 0	6	−0.3285	0.98
4 2 0	24	0.2070	0.92
5 1 0	24	−0.3994	1.0
4 4 0	12	0.2773	1.0
5 3 0	24	−0.3026	1.0
6 0 0	6	0.5253	1.04
4 4 2	24	−0.2423	0.97
5 3 2	48	0.2219	1.0
6 1 1	24	0.2208	1.07
6 2 2	24	−0.2594	0.96
7 2 1	48	0.1406	0.98
7 3 0	24	0.2657	1.0
7 5 2	48	−0.2333	1.0
9 3 2	48	−0.2128	1.0

[a] The legend is the same as for Table 2.

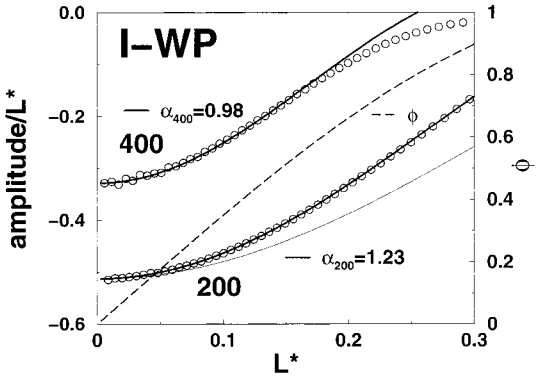

Figure 13. The I-WP surface. The amplitudes of the 200 and 400 reflections.

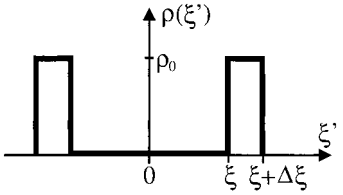

Figure 14. A model density profile for two thin layers of width $\Delta\xi$ laying in a constant distance ξ from the minimal surface. See text for explanation.

$$\Delta A(\mathbf{q}, \rho(\xi)) = F^{S}\frac{2\rho_0}{\alpha_{hkl}q}[\sin(\alpha_{hkl}q(\xi+\Delta\xi)) - \sin(\alpha_{hkl}q\xi)] \quad (21)$$

which for small $\Delta\xi$ can be approximated by

$$\Delta A(\mathbf{q}, \rho(\xi)) = F^{S}\frac{2\rho_0}{\alpha_{hkl}q}\frac{d}{d\xi}[\sin(\alpha_{hkl}q\xi)]\Delta\xi \quad (22)$$

And for $\Delta\xi \to 0$

$$dA(\mathbf{q}, l) = F^{S}2\rho(\xi)\cos(\alpha_{hkl}q\xi)\, d\xi \quad (23)$$

This last expression when integrated with a Kronecker delta distribution centered at distance ξ from the minimal surface can be compared with numerical evaluations of the scattering amplitudes for zero width parallel surfaces. This has been done by triangulating the parallel surfaces and evaluating an expression similar to the one for the SF (eq 10). This provides an alternative way of establishing the α parameters. In the case of all of seven explored structures, this test provided excellent agreement of the α correction parameters. However, as can be seen in Figure 15, the fits have a smaller range of applicability. The fits for the integral relation eq 19 work very well for the volume fractions up to $\phi \approx 0.8$ in the case of the P, D, and G structures and up to $\phi \approx 0.7$ in the case of the others. The differential relation is fitted well in the range of $\phi \in (0, 0.6)$.

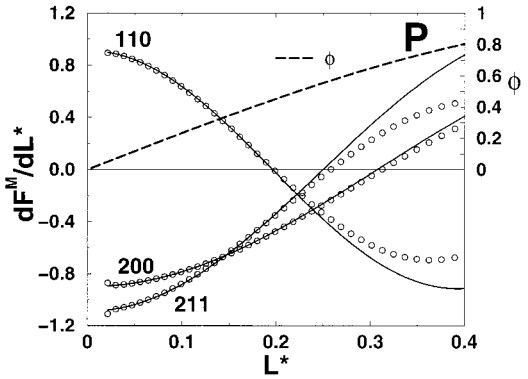

Figure 15. The numerically evaluated amplitudes for scattering on zero width parallel surfaces laying in distance $L/2$ away from the minimal surface are plotted with open circles. The solid lines correspond to the derivative of the molecular factor for uniform density profiles eq 23 with the same α correction parameters as the ones established by fitting the integral relation eq 19. As in the case of other structures, the fit for the differential relation works well for $\phi \in (0, 0.6)$ while the fit of eq 19 has a wider range of applicability $\phi \in (0, 0.8)$ for the P, D, and G structures and $\phi \in (0, 0.7)$ for the C(P), C(D), F-RD, and I-WP TPSs.

Having the expression eq 23 for the scattering amplitudes on parallel surfaces, we can reconstruct the scattering amplitude for any cross sectional density distribution $\rho(\xi)$ of the layer decorating the base minimal surface

$$A(\mathbf{q}, \rho(\xi)) = F^{S}2\int_0^\infty d\xi\, \rho(\xi)\cos(\alpha_{hkl}q\xi) \quad (24)$$

5. Debye−Waller Factor

The last effect that has to be accounted for is the fluctuations of the membrane. We will assume only fluctuations in the direction normal to the surface of the layer and no correlations between the fluctuation amplitudes. The first kind of fluctuations are those of a single molecule. Due to the amphiphilic forces that are responsible for separation of water and hydrocarbon-rich regions, the amplitude of the fluctuations of a single molecule is much smaller than the amplitude of the collective movements of the bilayer. We will parametrize both amplitudes by standard deviations σ_{single} and $\sigma_{\text{collective}}$. Since the total amplitude is

$$\sigma = (\sigma_{\text{single}}{}^2 + \sigma_{\text{collective}}{}^2)^{1/2} \quad (25)$$

in the first approximation, we can neglect the fluctuations of a single molecule.

To evaluate the impact of the fluctuations, we have assumed that they cause a broadening of the density profile described by a convolution of the original density profile $\rho(\xi)$ with a Gaussian distribution function with a standard deviation σ

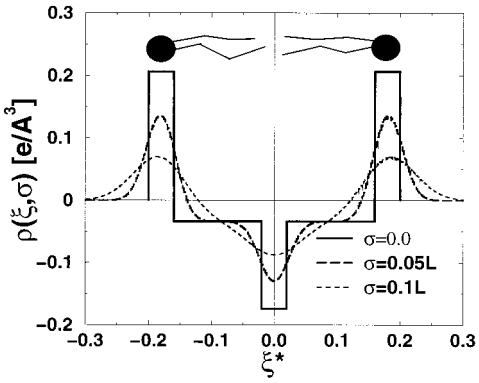

Figure 16. The cross sectional density profile used in the computations of Harper and Gruner[10] for a phospholipid molecule is shown with a solid line. The density distribution for fluctuations with amplitude parametrized by standard deviation $\sigma = 0.05L$ is shown with a dashed line, and $\sigma = 0.1L$ with a dotted line.

$$\rho_f(\xi, \sigma) = \frac{1}{\sigma(2\pi)^{1/2}} \int_{-\infty}^{\infty} d\xi' \, \rho(\xi') \exp\left[\frac{-(\xi - \xi')^2}{2\sigma^2}\right] \quad (26)$$

An example of such a broadening is presented in Figure 16. Since we already have a formula for the scattering on any density profile (eq 24), we can insert this broadened density distribution $\rho_f(\xi, \sigma)$ into eq 24 and obtain

$$A(\mathbf{q}, \rho(\xi), \sigma) = F^S \frac{2}{\sigma(2\pi)^{1/2}} \int_0^{\infty} d\xi \int_{-\infty}^{\infty} d\xi' \, \rho(\xi') \exp\left[\frac{-(\xi - \xi')^2}{2\sigma^2}\right] \cos(\alpha_{hkl} q \xi) \quad (27)$$

which after few analytical transformations can be expressed as Fourier transform of the Gaussian distribution leading to

$$A(\mathbf{q}, \rho(\xi), \sigma) = F^S [2 \int_0^{\infty} d\xi \, \rho(\xi) \cos(q\alpha_{hkl}\xi)] \exp\left[-\frac{1}{2}(q\alpha_{hkl}\sigma)^2\right] \quad (28)$$

We find that the influence of the fluctuations is independent of the original density profile $\rho(\xi)$. The Debye−Waller term is expressed in a very simple form

$$F^{DW}(\mathbf{q}, \sigma) = \exp\left[-\frac{1}{2}(q\alpha_{hkl}\sigma)^2\right] \quad (29)$$

Thus eq 28 is the final expression for the scattering amplitudes and it is exactly this formula which was presented as the general model (eq 2).

To inspect the influence of the Debye−Waller term, we have performed calculations for a detailed cross sectional density profile presented in the work of Harper et al.[10] The authors used the Fourier transform of the volume enclosed between parallel surfaces (to the base minimal surface) to compute the scattering amplitudes for a bilayer made of typical phospholipid molecules. The width of the headgroup layer was set to 2/10 of the monolayer width ($L/2$). The hydrocarbon tail length was 7/10 of $L/2$, and finally the terminal methyl groups were said to occupy a layer of width equal to 1/10 of $L/2$. The electron densities were 0.54, 0.3, and 0.16 e/Å^3, respectively. After the electron density of water (0.33e/Å^3) was subtracted, the relative densities were 21/−3/−17 for head/tail/methyl groups, Figure 16. Figure 17 shows the influence of the fluctuations on the scattering amplitudes for a D TPMS

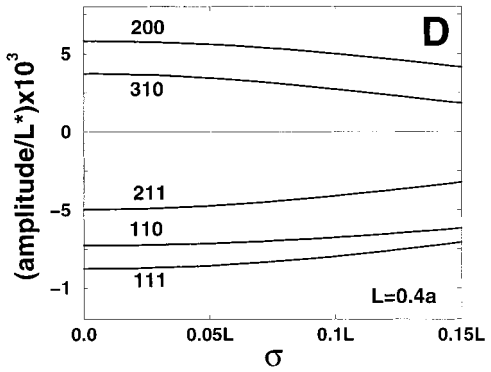

Figure 17. The impact of the fluctuations on the scattering amplitudes of the D TPMS based phase with a cross sectional density profile shown on Figure 16.

based cubic phase. It is in agreement with our previous work[13] that the decrease of the intensity of the Bragg reflections associated with fluctuations is small. Even for large fluctuations of amplitude $\sigma = 0.1L$ (see Figure 16), the decrease of the intensity is on the order of 10−20%. At the same time the dependence on the layer width is much stronger. For example the intensity ratio of the 211 peak to the 110 peak of the P TPMS based phase is $I_{211}/I_{110} = 1.6$ for the volume fraction $\phi = 0.3$ and $I_{211}/I_{110} = 0.2$ for $\phi = 0.7$.

6. Summary

The results of this paper are summarized in eqs 2 and 5 and Tables 2−8. The first equation enables reconstruction of the scattering amplitudes for any electron density profile and fluctuations. A detailed cross sectional density profile can be constructed from the knowledge of the microscopic details of the molecules present in the system. Then it can be tested by comparing the amplitudes evaluated through eq 2 with high-quality experimental diffraction data.

For a simpler and faster analysis, we propose modeling described by eq 5. It takes into account only the crude (eq 11) electron density contrast and neglects the fluctuations. The last point has been justified in section 5. The Heaviside distribution form of the density function is related to the fact that the main contrast in most amphiphilic systems results from the electron density difference of water and hydrocarbons.

In the following article we will show that even such a crude model provides crucial information on the type of the structure, its microscopic details, and the stability of the system. Namely, in phase coexisting systems, one can determine the phases present, their structural relationships, volume ratios, etc. In time-resolved techniques, this could lead into an interesting insight on the kinetics and mechanisms of phase transitions.

Furthermore this approach could be used to study how the amplitude signs change with the parameters for more detailed density profiles. In this respect our approach could be used together with the method presented in ref 10 in order to find simple formulas for the intensity and density distribution in surfactant systems leading to reconstruction of the actual density map of the cubic phases in amphiphilic systems.

Acknowledgment. We thank Dr. Marcin Fiałkowski for helpful discussions. This work has been supported by the KBN Grants 5 P03B 094 21 (2001−2003) and 5 P03B 084 21 (2001−2002).

LA011298P